The role of sea ice in the fresh water budget of the Weddell Sea

R. Timmermann, A. Beckmann, H.H. Hellmer
Alfred Wegener Institute for Polar and Marine Research, Germany

Abstract

A coupled sea ice-ocean model of the Weddell Sea has been developed as part of the BRIOS (Bremerhaven Regional Ice-Ocean Simulations) project. It is based on the s-Coordinate Primitive Equation ocean Model (SPEM) and a dynamic-thermodynamic sea ice model with viscous-plastic rheology which also provides the thermohaline forcing at the base of the Antarctic ice shelves. Model runs are forced with wind, cloudiness, temperature and precipitation fields of the ECMWF and NCEP reanalyses. Model results show a good agreement with observations of ice extent, thickness and drift. Water mass properties and the large scale circulation are in good agreement with observations. Fresh water fluxes from sea ice formation as well as from ice shelf basal melting, and from precipitation are computed and compiled to the fresh water budget of the Weddell Sea. Supporting estimates based on hydrographic observations, model results indicate that fresh water loss due to sea ice formation and export (34 mSv) is roughly balanced by ice shelf basal melting (9 mSv) and net precipitation (19 mSv). Furthermore, sea ice formation appears as a necessary condition for bottom water production in the Weddell Sea.

Introduction

Seasonal variations of sea ice cover in the Southern Ocean represent one of the most pronounced signals in the annual cycle of the world climate system. Intense cooling and brine rejection during sea ice formation in the southwestern Weddell Sea lead to an increase in density of the water masses on the continental shelf. Mixing of this High Salinity Shelf Water (HSSW) with Modified Warm Deep Water (MWDW) yields Weddell Sea Bottom Water (WSBW; Foster and Carmack, 1976), which contributes to the formation of Antarctic Bottom Water that spreads into the world ocean.

As density of high latitude sea water is strongly controled by salinity, the fresh water budget of this region plays a key role in determining the characteristics of the newly formed water masses. For the Weddell Sea, formation and northward drift of sea ice yield an export of fresh water and thus are crucial to the salinity enrichment. Sources of fresh water are basal melting of ice shelves and the difference between precipitation and evaporation. Based on experiments with a newly developed coupled ice-ocean model, this paper presents an estimate of the surface fresh water balance of the inner Weddell Sea (i.e. the region south of the line Kapp Norvegia - Joinville Island) and addresses the impact of sea ice formation on water mass characteristics in the Weddell Sea.

Model Configuration

The coupled sea ice-ocean model applied to this study is called BRIOS-2 and is based on a hydrostatic regional ocean circulation model and a dynamic-thermodynamic sea ice model which is also applied to ice shelf-ocean interaction.

The hydrostatic primitive equation model SPEM (Haidvogel and others, 1991) with a generalized s-coordinate transformation (Song and Haidvogel, 1994) was chosen because its terrain-following vertical coordinate is well suited for studies in model domains with both shallow and deep regions. Modifications allowing for the inclusion of sub-ice shelf cavities as well as the subgrid-scale parameterizations developed for both the stand-alone ocean model BRIOS-1 and the coupled model BRIOS-2 are described by Beckmann and others (1999).

The dynamic-thermodynamic sea ice model includes a viscous-plastic rheology (Hibler, 1979), the Parkinson and Washington (1979) thermodynamics using the Semtner (1976) zero-layer approach for heat conduction, and a prognostic snow layer (Owens und Lemke, 1990) accounting for the effect of snow-ice conversion in case of flooding (Leppäranta, 1983; Fischer, 1995). As a stand-alone sea ice model, it has been used for a sea ice-mixed layer-atmosphere interaction study in the Weddell Sea (Timmermann et al., 1999) as well as to provide the forcing data for the stand-alone ocean model BRIOS-1 in a circumpolar model domain (Beckmann et al., 1999). In this study, the model's thermodynamic component is also applied to the ice-ocean interaction at the ice shelf base. In the entire model domain, freezing temperature is a function of pressure and salinity. While this does not significantly affect sea ice-ocean interaction it is essential for the description of sub-ice shelf processes (see, e.g., Hellmer and Olbers, 1989).

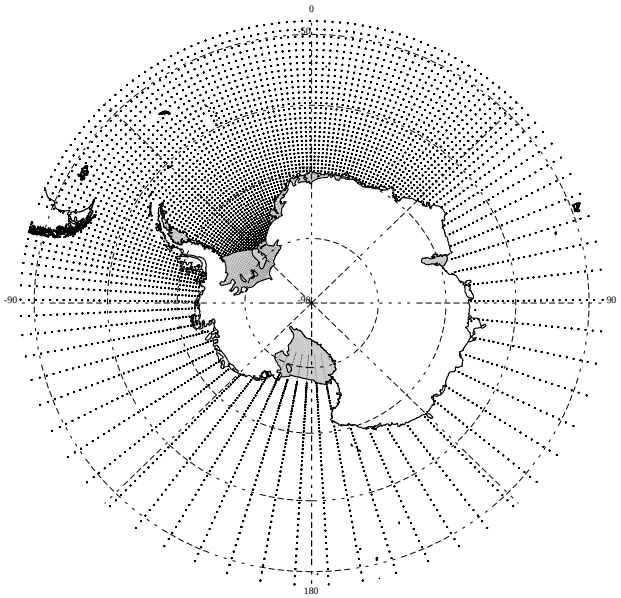

Figure 1. BRIOS-2 model grid. Bold marks denote open ocean; smaller marks on shaded areas indicate sub-ice shelf grid points.

The integration is carried out on a circumpolar grid between 82°S and 48°S (Fig. 1). It covers the whole Southern Ocean but is focused on the Weddell Sea where the resolution is isotropic (1.5° in the zonal, 1.5°cosΦ in the meridional direction). In the vertical, 24 levels are used with increasing resolution near the surface and the bottom. Bottom topography was derived from data of Smith and Sandwell (1997), Johnson and Smith (1997) and Schenke and others (1998). Filchner-Ronne and Ross Ice Shelf thicknesses are derived from the dataset of Johnson and Smith (1997); the thickness of all other ice shelves is assumed to be 200 m owing to a lack of detailed data. At the open northern boundary, temperature and salinity are restored to climatological fields from the Hydrographic Atlas of the Southern Ocean (HASO; Olbers

and others, 1992). The transport of the ACC through Drake Passage is prescribed to be 130 Sv.

Model runs are initialized using data from HASO and forced with 6-hourly data of 10 m-wind, total cloudiness and 2 m-air and dew point temperature from the ECWMF reanalyses of 1985-1993. Precipitation and evaporation rates are derived from the NCEP reanalysis dataset. Two passes of this nine year period are used to obtain a quasi-stationary seasonal cycle of the sea ice distribution. Results presented in this paper are from the third 9 years of integration.

The model has been validated with respect to minimum and maximum ice extent (presented below), ice thickness, and drift using SSM/I, Upward Looking Sonar (ULS) and buoy drift data. A prominent feature of the simulated ocean circulation is a pronounced double cell structure quite similar to the results of Beckmann and others (1999) with transports quantitatively consistent with measurements of Fahrbach and others (1994) and Schröder and Fahrbach (1999). Water mass properties will be shown to be in good agreement with observations. A more complete description of this model and its validation is part of a separate paper currently in preparation. Here, we focus on freezing and melting of sea ice and ice shelves and the related fresh water fluxes.

Model Results and Discussion

Freezing and melting of sea ice

Indicative of the coupled model's seasonal cycle are minimum and maximum sea ice extent in the Weddell Sector of the Southern Ocean (Fig. 2). It appears that the model tends to underestimate the summer sea ice coverage especially in the northwestern Weddell Sea. Sensitivity studies using the ECMWF *analysis* instead of the *reanalysis* data indicate that due to the coarser resolution in the reanalysis the topographic effect of the Antarctic Peninsula is not adequately covered. Compared to the *analysis*, 2 m-temperatures in the ECMWF *reanalysis* in that region are warmer by 1 to 2 °C, thus warmer than the ocean surface freezing temperature. This leads to a downward flux of sensible heat causing unrealistic melting of sea ice in that part of the model domain.

In contrast, the maximum sea ice extent is in good agreement with observations. Winter sea ice coverage is predominantly determined by the effects of the west wind drift and the Antarctic Circumpolar Current (ACC) which (1) acts as a force driving sea ice eastward and (2) forms a "thermal barrier" limiting further northward spreading of ice.

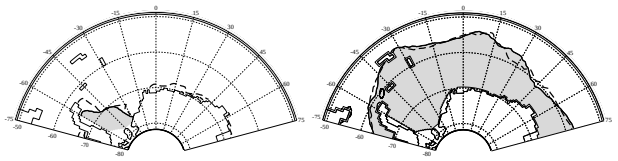

Figure 2. Simulated minimum (left) and maximum (right) sea ice extent (as defined by the 15% ice concentration isoline) in the Weddell Sea, derived from monthly means of February and September 1987, respectively. Dashed lines indicate the respective observed sea ice coverage, derived from the PELICON analyses (Heygster and others, 1996). Modeled ice cover is shaded.

Due to regional differences in the heat balance of the upper ocean, freezing and melting regions of sea ice do not coincide. Between formation and decay, sea ice may drift over distances of more than 1000 km. In the 9-year average, the highest net freezing rates (typically 1.5-2 m/yr, maximum up to 4 m/yr in the southwestern Weddell Sea) occur along the Antarctic coast (Fig. 3). Katabatic winds in these regions induce a divergent ice drift and carry very cold continental air. In reality, they lead to the formation of coastal polynyas in which great amounts of sea ice are formed (Markus and others, 1998). The model is not able to resolve these polynyas as open water grid boxes but it does reproduce the divergent ice drift causing low sea ice concentrations, increased heat loss in the open water areas, and thus the high freezing rates along the coast.

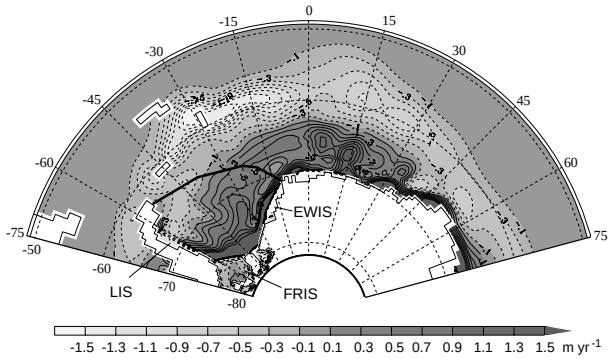

Figure 3. Net freezing rates, averaged over nine years of integration. Contour interval is 0.2 m/yr. Dashed contour lines indicate negative net freezing rates, i.e., melting. The wave-like structure in the western Weddell Sea is an artefact of averaging and has no physical significance. The solid black line represents the line Kapp Norvegia - Joinville Island and thus the northern boundary of the inner Weddell Sea. Ice Shelves: FRIS = Filchner-Ronne Ice Shelf, LIS = Larsen Ice Shelf, EWIS = Eastern Weddell Ice Shelves.

Clearly separated from the sea ice formation regions are the regions of net melting. The highest melting of up to 1.8 m/yr occurs arround 60°S where the sea ice encounters the warm surface waters of the ACC.

The model has been validated using ice thickness data derived from measurements of six Upward Looking Sonars (ULS; Strass and Fahrbach, 1998) which were moored along the line Kapp Norvegia – Joinville Island in the Weddell Sea (see Fig. 3). Comparison of simulated sea ice thickness with the observed 7 day-mean yields an underestimation of short term variability but shows a good agreement with winter ice thickness in the central and eastern Weddell Sea. However, as summer sea ice melting in the northwestern Weddell Sea is overestimated, the model tends to underestimate sea ice volume in the vicinity of the Antarctic Peninsula. Export of sea ice across the line Kapp Norvegia – Joinville Island, i.e., net ice export out of the inner Weddell Sea, in the period 1985–1993 was estimated to be $(46 \pm 8) \cdot 10^3$ m^3 s^{-1} by Harms and others (1999). The simulated 9-year average ice export out of the inner Weddell Sea is $(42 \pm 26) \cdot 10^3$ m^3 s^{-1} which is quite close to the estimates derived from observations. Assuming the sea ice salinity to be 5 psu and densities of 910 kg/m^3 for sea ice and 290 kg/m^3 for snow this converts into a fresh water export of 33.7 mSv (1 mSv $= 10^3$ m^3 s^{-1}), which is extracted from the inner Weddell Sea surface by the formation of sea ice and the accumulation of snow.

Freezing and melting of ice shelves

As can be seen in Fig. 3, freezing and melting rates at the ice shelf base can be of the same order of magnitude as the net freezing rates of sea ice. Under the Filchner-Ronne Ice Shelf (FRIS), the highest melting rates of up to 3 m/yr occur near the grounding line, where the *in situ* freezing temperature is as low as -2.6°C (Fig. 4). Basal melting rates over the Filchner Depression reach 1.5 m/yr. North of the combined Henry/Korff Ice Rise Complex, a large area with basal freezing rates of 0.3 m/yr is encountered. Compared with the FRIS model of Gerdes and others (1999) who use a higher resolution but fixed northern boundary conditions, the distribution of basal freezing and melting regions is quite similar. In their model, the basal freezing region north of Henry/Korff Ice Rise is significantly smaller but this is compensated for by a higher freezing rate. Further difference exists for the melting rates at the Filchner Ice Shelf base, which are significantly less pronounced in the Gerdes and others' model. Using the ice shelf model of Hellmer and others (1998) for the Filchner-Ronne Ice Shelf (as described by Beckmann and others, 1999) yields lower amplitudes of both freezing and melting, but an average melting rate between 29 and 30 cm/yr is computed in both models resulting in a mean net fresh water input of 3.2 mSv.

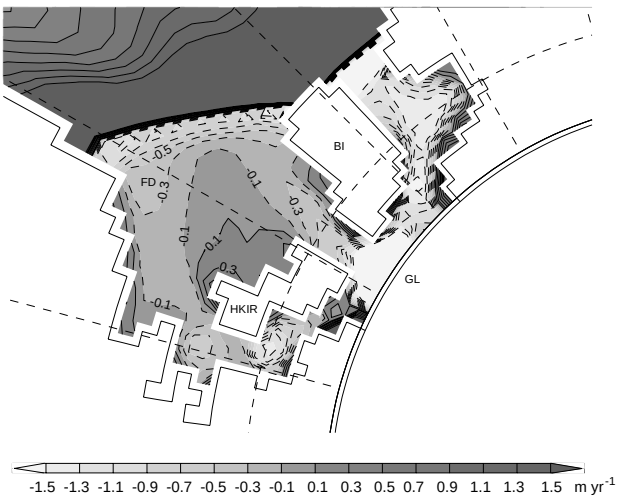

Figure 4. As in Fig. , but zoomed into FRIS region. HKIR = Henry/Korff Ice Rise, BI = Berkner Island; FD = Filcher Depression, GL = grounding line.

Ice-ocean interaction at the base of Larsen Ice Shelf (LIS) and the Eastern Weddell Ice Shelves (EWIS) is characterized by high melting rates. In the EWIS cavity, relatively warm water from the coastal current is in direct contact with the ice shelf base. Beneath LIS, no water warmer than -1.2°C is found in the simulation. Since this is still warmer than the -1.6°C observed by Gordon (1998), freezing rates might be overestimated. However, it is reasonable to believe that near the grounding line both ice shelves are thicker than the 200 m prescribed in the model. Keeping that in mind, the temperature difference between the uppermost layer and the ice shelf base might well be captured realistically.

In BRIOS-2, LIS and EWIS yield fresh water fluxes of 1.6 and 4.2 mSv, respectively. Thus, despite their small extent, the Eastern Weddell Ice Shelves provide more fresh water than the much larger Filchner-Ronne Ice Shelf.

Fresh Water budget of the inner Weddell Sea

In the previous sections we discussed ice-ocean interactions in the inner Weddell Sea and introduced the resulting fresh water fluxes. Combining these components leads us to an estimate of the surface fresh water balance of the inner Weddell Sea.

In the nine-year average, sea ice formation and export extracts 33.7 mSv of fresh water from the inner Weddell Sea. Ice shelf basal melting provides 9.1 mSv of fresh water, net precipitation (precipitation minus evaporation from NCEP reanalysis) adds another 19.0 mSv (Fig. 5).

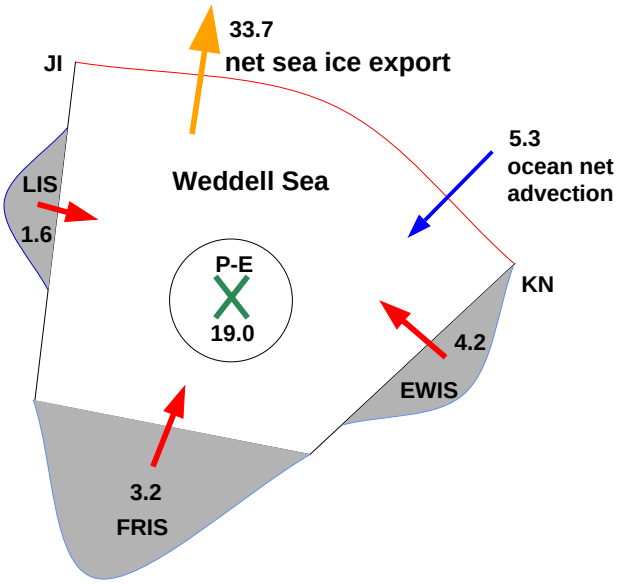

Figure 5. Fresh water budget of the inner Weddell Sea, derived from the 9 year-average simulated fresh water fluxes [mSv] in BRIOS-2. JI = Joinville Island, KN = Kapp Norvegia; LIS = Larsen Ice Shelf, FRIS = Filchner-Ronne Ice Shelf, EWIS = Eastern Weddell Ice Shelves.

More fresh water originates from the Antarctic continent. According to Huybrechts (pers. communication), fresh water runoff from the Antarctic continent does not exceed $10 \cdot 10^{12}$ kg/yr, which results in a circumpolar fresh water input below 0.3 mSv and an estimated 0.05 mSv for the inner Weddell Sea which is clearly negligible. The maximum estimate for iceberg calving amounts to $2000 \cdot 10^{12}$ kg/yr which would yield roughly 60 mSv for the entire Southern Ocean. However, since most of the iceberg melting occurs north of 65°S when in contact with the warm waters of the ACC (Romanov, 1974), this contribution can be neglected as well. Snow accumulated on top of the ice shield and shelves may be carried into the open ocean by catabatic winds. As reliable estimates of the drifted snow volume do not exist we ignore this contribution.

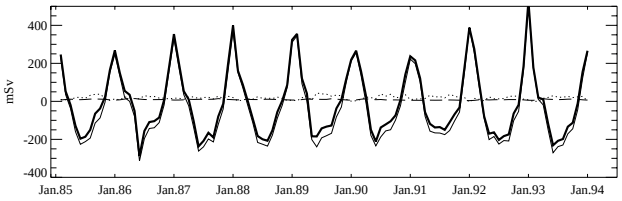

Figure 6. Time series of monthly mean fresh water fluxes from sea ice formation (solid), basal melting of ice shelves (dashed) and net precipitation (dotted) and the overall surface fresh water fluxes in the inner Weddell Sea (bold). 1 mSv = 10^3 m^3/s.

The balance from all fresh water fluxes considered here reveals that fresh water extraction by sea ice formation is roughly counterbalanced by the input through net precipitation and shelf ice basal melting in the annual mean. For the 9-year average, 5.3 mSv of fresh water are extracted through the surface of the inner Weddell Sea. However, time series of these fresh water fluxes (Fig. 6) indicate that the net amount is the residuum of several large components of different signs. In the annual cycle, the monthly mean fresh water input varies between -200 und 400 mSv. Seasonal variability is dominated by freezing and melting of sea ice. The influence of fluctuations of net precipitation and ice shelf melting is minor. The standard deviation of the annual mean net surface fresh water flux is 13 mSv and thus much larger than the 9 year-average.

The fresh water budget of the inner Weddell Sea as we derived it from model analysis is quite close to the mostly remote-sensing data based estimate of Drinkwater and others (this issue). However, considering the large standard deviation in the annual mean net surface fresh water flux, these results do not conflict with estimates of Fahrbach and others (1994), pointing out that the net (southward) advection of salt into the inner Weddell Sea is not significantly different from zero.

Sensitivity of water mass structure in the Weddell Sea to sea ice-related salt fluxes

In contrast to a number of previous coupled sea ice-ocean models (e.g., Kim and Stössel, 1998), bottom water formation in BRIOS-2 does not occur through deep convection in the central Weddell Sea. Instead, the application of an ocean circulation model with terrain-following vertical coordinate enables us to cover processes on the continental shelf quite realistically, and an adequat parametrization of vertical mixing (Beckmann and others, 1999) prevents the water column in the central Weddell Sea from being homogenized. Thus, simulated water mass characteristics in the Weddell Sea (Fig. 7 left) are in good agreement with observations presented by Schröder and Fahrbach (1999). Specifically, High Salinity Shelf Water (HSSW) with $S > 34.75$ and temperature near the freezing point (T_f) is formed on the continental shelf of the southwestern Weddell Sea. Its presence, however, is subject to seasonal and interannual variability.

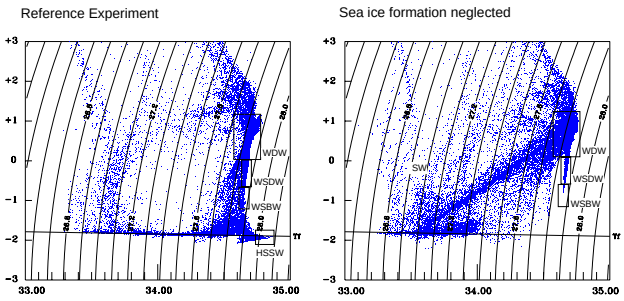

Figure 7. Simulated monthly mean Θ-S-diagrams of August 1993 derived from grid points outside the ice shelf cavities in the reference experiment (left) and a simulation with all sea ice-related salt fluxes neglected (right). The solid line indicates the surface freezing temperature (T_f) as a function of salinity.

In order to investigate the effect of sea ice formation on the water mass structure, we performed an experiment in which all salt fluxes related to sea ice growth and decay were eliminated. Once the ocean surface reaches freezing temperature further heat loss is excluded. From the heat flux point of view, this resembles a zero order sea ice model like the approach often used in ocean modelling (e.g., DYNAMO Group, 1997).

Ignoring the surface salt flux leads to a rapid change in the water mass structure (Fig. 7 right). No more High Salinity Shelf Water (HSSW) is formed; instead Warm Deep Water (WDW) mixes with lighter Surface Water (SW) which became fresher by 1 psu within 5 years of integration. Due to an insufficient density increase, mixed layer deepening in autumn is greatly reduced; a pronounced winter water layer does not form and mixing of WDW and SW occurs mainly as cross-pycnocline diffusion driven by the strong vertical gradients. No water denser than the Warm Deep Water (WDW) is formed at any time of the year, thus the bottom water is not ventilated any more and even the large amount of Weddell Sea Deep Water (WSDW) is slowly eroded. This leads us to conclude that sea ice formation over the continental shelf in the southwestern Weddell Sea is a necessary condition for formation of Weddell Sea Deep and Bottom Water.

Conclusions

The fresh water budget of the inner Weddell Sea, i.e. the region south of the line Kapp Norvegia – Joinville Island, is dominated by the balance between fresh water removal due to sea ice formation and export, and fresh water input by ice shelf basal melting and net precipitation. The net amount of fresh water loss through the surface of the inner Weddell Sea is estimated to be 5 ± 13 mSv in the annual mean and thus not significantly different from zero.

Sea ice formation appears to be a necessary condition for the formation of Weddell Sea's deep and bottom waters and thus for the renewal of Antarctic Bottom Water ventilating the world ocean.

Since stratification in the Weddell Sea is weak, any changes in the sea ice formation and the surface fresh water balance might influence the onset of deep convection, have a significant impact on water mass formation and thus affect the global thermohaline circulation.

Acknowledgements

The authors would like to thank W. Cohrs and C. Lichey for preparing the ECMWF and NCEP atmospheric forcing fields which were received via the German Weather Service (Deutscher Wetterdienst, DWD) and the NOAA-CIRES Climate Diagnostics Center, Boulder, using the website http://www.cdc.noaa.gov/, respectively.

References

Beckmann, A., H. H. Hellmer and R. Timmermann. 1999. A numerical model of the Weddell Sea: large scale circulation and water mass distribution. *J. Geophys. Res.*, **104(C10)**, 23375-23391.

Drinkwater, M.R., X. Liu and S. Harms. 2000. Combined satellite- and ULS-derived sea-ice flux in the Weddell Sea. *Annals of Glaciology* (this issue).

DYNAMO Group. 1997. Dynamics of North Atlantic Models: Simulation and assimilation with high resolution models. *Berichte aus dem Institut für Meereskunde*, Christian-Albrechts-Universtität, Kiel, 334 pp.

Fahrbach, E., G. Rohardt, M. Schröder and V. Strass. 1994. Transport and structure of the Weddell Gyre. *Annales Geophysicae*, **12**, 840-855.

Fischer, H. 1995. Vergleichende Untersuchungen eines optimierten dynamisch-thermodynamischen Meereismodells mit Beobachtungen im Weddellmeer. *Berichte zur Polarforschung* **166**, Alfred-Wegener-Institut (AWI), Bremerhaven, 130 pp.

Foster, T. D. and E. C. Carmack. 1976. Frontal zone mixing and Antarctic Bottom Water formation in the southern Weddell Sea. *Deep Sea Res.*, **23(4)**, 301-317.

Gerdes, R., J. Determann and K. Grosfeld. 1999. Ocean circulation beneath Filchner-Ronne Ice Shelf from three-dimensional model results. *J. Geophys. Res.*, **104(C7)**, 15827-15842.

Gordon, A.L. 1998. Western Weddell Sea thermohaline stratification. In *Ocean, Ice and Atmosphere: Interactions at the Antarctic Continental Margin.*

Antarct. Res. Ser., **75**, edited by S. S. Jacobs and R. F. Weiss, 215-240, AGU, Washington, D.C.

Haidvogel, D.B., J. L. Wilkin and R. E. Young. 1991. A semi-spectral primitive equation ocean circulation model using vertical sigma and orthogonal curvilinear horizontal coordinates. *J. Comput. Phys.*, **94**, 151-185.

Harms, S., E. Fahrbach and V. H. Strass. 1999. Ice transport in the Wedell Sea. *J. Geophys. Res.*, (submitted).

Hellmer, H. H. and D. Olbers. 1989. A two-dimensional model for the thermohaline circulation under an ice shelf. *Antarctic Science*, **1**, 325-336.

Hellmer, H. H., S. S. Jacobs and A. Jenkins. 1998. Oceanic Erosion of a floating glacier in the Amundsen Sea. In: *Ocean, Ice and Atmosphere: Interactions at the Antarctic Continental Margin, Antarctic Research Series*, **75**, 83-99.

Heygster, G., L. T. Pedersen, J. Turner, C. Thomas, T. Hunewinkel, H. Schottmüller and T. Viehoff. 1996. PELICON: Project for estimation of long-term variability of ice concentration. *EC Contract Report* EV5V-CT93-0268 (DG 12), Bremen.

Hibler, W. D., III. 1979. A dynamic thermodynamic sea ice model. *J. Phys. Oceanogr.*, **9(4)**, 815-846.

Johnson, M. R., and A. M. Smith. 1997. Seabed topography under the southern and western Ronne Ice Shelf, derived from seismic surveys. *Antarctic Science*, **9(2)**, 201-208.

Kim, Seong-Joong and A. Stössel. 1998. On the representation of the Southern Ocean water masses in an ocean climate model. *J. Geophys. Res.*, **103(C11)**, 24891-24906.

Leppäranta, M. 1983. A growth model for black ice, snow ice, and snow thickness in subarctic basins. *Nordic Hydrology*, **14**, 59-70.

Markus, T., Ch. Kottmeier and E. Fahrbach. 1998. Ice Formation in coastal polynyas in the Weddell Sea and their impact on oceanic salinity. In: *Antarctic Sea Ice: Physical Processes, Interactions and Variability, Antarctic Res. Ser.*, **74**, edited by M. O. Jeffries, 273-292.

Olbers, D., V. Gouretski, G. Seiss and J. Schröter. 1992. Hydrographic atlas of the Southern Ocean. Alfred Wegener-Institut für Polar- und Meeresforschung, Bremerhaven.

Owens, W. B. and P. Lemke. 1990. Sensitivity studies with a sea ice-mixed layer-pycnocline model in the Weddell Sea. *J. Geophys. Res.*, **95(C6)**, 9527-9538.

Parkinson, C. L. and W. M. Washington. 1979. A large-scale numerical model of sea ice. *J. Geophys. Res.*, **84(C1)**, 311-337.

Romanov, A. A. 1974. The size of icebergs in east Antarctica. *Sov. Antarct. Exped. Inf. Bull.*, **8**(9), 499-500.

Schenke, H.W., H. Hinze, S. Dijkstra, B. Hoppmann, F. Niederjasper, and T. Schöne. 1998. The new bathymetric charts of the Weddell Sea: AWI BCWS. In: *Ocean, Ice and Atmosphere: Interactions at the Antarctic Continental Margin. Antarctic Research Series*, **75**, edited by S. S. Jacobs and R. F. Weiss, 373-382, AGU, Washington D.C.

Schröder, M. and E. Fahrbach. 1999. On the structure and the transport of the eastern Weddell Gyre, *Deep-Sea Res.*, Ser. II, **46**(1-2), 501-527.

Semtner, A. J., Jr. 1976. A model for the thermodynamic growth of sea ice in numerical investigations of climate. *J. Phys. Oceanogr.*, **6(3)**, 379-389.

Smith, W.H.F., and D.T. Sandwell. 1997. Global sea floor topography from satellite altimetry and ship depth soundings. *Science*, **277**(5334), 1956-1962.

Song, Y., and D.B. Haidvogel. 1994. A semi-implicit ocean circulation model using a generalized topography-following coordinate. *J. Comput. Phys.*, **115**, 228-244.

Strass, V. H. and E. Fahrbach. 1998. Temporal and regional variation of sea ice draft and coverage in the Weddell Sea obtained from Upward Looking Sonars. In: *Antarctic Sea Ice: Physical Processes, Interactions and Variability, Antarctic Res. Ser.*, **74**, edited by M. O. Jeffries, 123-139.

Timmermann, R., P. Lemke and Ch. Kottmeier. 1999. Formation and maintenance of a polynya in the Weddell Sea. *J. Phys. Oceanogr.*, **29(6)**, 1251-1264.

This preprint was prepared with AGU's LaTeX macros v4. File igspap formatted July 31, 2000.